Catalysis Today 155 (2010) 101–107

Contents lists available at ScienceDirect

Catalysis Today

journal homepage: www.elsevier.com/locate/cattod

Rh-based catalysts for syngas production via SCT-CPO reactors

S. Specchia [a,*], L.D. Vella [a], L. De Rogatis [b], T. Montini [b,c], V. Specchia [a], P. Fornasiero [b,c]

[a] Dipartimento di Scienza dei Materiali ed Ingegneria Chimica, Politecnico di Torino, Corso Duca degli Abruzzi 24, 10129 Trieste, Italy
[b] Dipartimento di Scienze Chimiche and INSTM-Trieste, Università di Trieste, Via L. Giorgieri 1, 34127 Trieste, Italy
[c] ICCOM-CNR Unità di Ricerca di Trieste, Via L. Giorgieri 1, 34127 Trieste, Italy

ARTICLE INFO

Article history:
Available online 19 May 2009

Keywords:
Syngas production
Methane catalytic partial oxidation
Short time contact
Fixed bed reactor
Rhodium catalyst
Alumina carrier
Egg-shell/egg-yolk catalyst type

ABSTRACT

Short contact time catalytic partial oxidation (SCT-CPO) of natural gas is a promising technology for syngas production, representing an appealing alternative to existing processes. This process is likely to become more important in the future due to its advantages in thermodynamics, mildly exothermic overall reaction, H_2/CO ratio of 2, ideal for downstream processes. The present work refers to an experimental study of syngas production from CH_4 and O_2 via a SCT-CPO reactor made of a fixed bed of Rh/Al_2O_3 spheres, with Rh deposited in egg-shell or egg-yolk configuration. In the WHSV range from 120 to 470 Nl h^{-1} g_{cat}^{-1}, five different fixed bed structures were investigated. The best performances in term of CH_4 conversion and H_2 selectivity, together with no coke formation, were obtained with an physical mixture of egg-shell and egg-yolk catalysts at WHSV values of 150–300 Nl h^{-1} g_{cat}^{-1}.

1. Introduction

Partial oxidation is presently considered an alternative to steam reforming for the generation of H_2 from fossil fuels in decentralized applications [1]. An important recent example is the generation of H_2 for stationary or mobile fuel cells [2]. The catalytic partial oxidation (CPO) of CH_4 to CO/H_2 mixtures has been discussed in the literature and several catalysts were proposed, including non-noble [3–5] and noble metals-based ones [6–9]. The extensive work on short contact time (SCT) reactors available in literature [10–28] showed that Rh has high activity and selectivity, superior to that of other noble metals, avoiding or at least partially limiting coke formation [29]. The use of Rh leads to the conversion of CH_4/O_2 mixtures to CO and H_2 at contact times of few milliseconds under adiabatic conditions (e.g., at temperatures higher than 800 °C [22]).

It is widely accepted that with metal catalysts CH_4 is first oxidized to CO_2 and H_2O in the initial part of the catalytic bed until O_2 is exhausted [30]; then, in the following part of the bed, the reforming reactions of remaining CH_4 with steam and CO_2 initially formed [6–8] occur. However, at extremely high temperatures and very short contact time, syngas may be formed directly [7,8,11–13]. The main chemical reactions involved in the catalytic process are represented in Eqs. (1)–(6):

Methane total oxidation (MTO):

$$CH_4 + 2O_2 \rightarrow CO_2 + 2H_2O, \quad \Delta H_{298}^{\circ} = -802.3\,kJ\,mol^{-1} \qquad (1)$$

Methane partial oxidation (MPO):

$$CH_4 + 1/2O_2 \rightarrow CO + 2H_2, \quad \Delta H_{298}^{\circ} = -35.7\,kJ\,mol^{-1} \qquad (2)$$

Methane steam reforming (MSR):

$$CH_4 + 2H_2O \rightarrow CO + 3H_2, \quad \Delta H_{298}^{\circ} = 206.2\,kJ\,mol^{-1} \qquad (3)$$

Methane dry reforming (MDR):

$$CH_4 + CO_2 \rightarrow 2CO + 2H_2, \quad \Delta H_{298}^{\circ} = 247.3\,kJ\,mol^{-1} \qquad (4)$$

Water gas shift equilibrium (WGS):

$$CO + H_2O \leftrightarrow CO_2 + H_2, \quad \Delta H_{298}^{\circ} = -41.1\,kJ\,mol^{-1} \qquad (5)$$

Coke formation (Boudouard reaction):

$$2\,CO \rightarrow CO_2 + C, \quad \Delta H_{298}^{\circ} = -172.9\,kJ\,mol^{-1} \qquad (6)$$

The effect of catalyst preparation and pretreatment, as well as of Rh precursors and of the carriers over the morphology of Rh nanoparticles was also investigated [31–40]: both metallic Rh particles and highly dispersed Rh species were found to be active towards CPO; their relative amount can change following the exposition to the high temperature of the CH_4 CPO conditions [37]. The exposition of the catalysts to high temperatures induced a reconstruction of the surface, since its heterogeneity was largely

* Corresponding author. Tel.: +39 011 0904608; fax: +39 011 0904699.
E-mail address: stefania.specchia@polito.it (S. Specchia).

0920-5861/$ – see front matter © 2009 Elsevier B.V. All rights reserved.
doi:10.1016/j.cattod.2009.04.008

eliminated and the reorganization of isolated atoms and the smaller aggregates into bigger metallic particles occurred [38,39]. Recently, Rh embedded into porous Al_2O_3 has been shown promising stability performances [41,42].

The present work deals with the experimental activities on SCT-CPO of CH_4 on a fixed bed reactor of Rh-supported alumina particles; a set of experimental data, related to CH_4 conversion (ξ_{CH_4}), H_2 and CO selectivity (σ_{H_2} and σ_{CO}), mainly focusing on the effects of weight hourly space velocity (WHSV), is presented and discussed. The goal of this work was the design of an optimal fixed bed structure, in order to attain a very thermally stable system under extreme working conditions, avoiding sintering and coking problems, using two different kinds of 1 wt.% Rh on Al_2O_3 catalysts, alone or in combination: one catalyst carrying Rh on the external support surface (egg-shell) and the other with Rh embedded into the support pores (egg-yolk).

For the egg-shell catalyst, the metallic active phase is distributed only on a thin external surface layer (about 50 μm thick) of γ-Al_2O_3 carrier spheres, but not in the internal pores. Such a situation is congruent with a low contact time process which is controlled by external mass transfer phenomena [43]: the reaction takes place on the catalyst surface, easily and quickly accessible by the reagents, which would have limited possibility to diffuse and react inside the pores. Anyway, the idea to study also an egg-yolk configuration, i.e., to embed Rh nanoclusters in porous Al_2O_3, was born to limit the sintering of Rh clusters under the severe MPO environment [40,41]. Moreover, the porous structure of Al_2O_3 wrapping Rh nanoparticles should control the diffusion rate of the reactant molecules inside the carrier: Knudsen type diffusion mechanism of the reactant molecules has been proposed for microporous γ-Al_2O_3 [44]. In this case, a diffusion rate of a reactant molecule is faster as its molecular weight becomes smaller.

2. Experimental

The egg-shell Rh catalyst, hereafter named catalyst "*A*", was prepared by Rh deposition over commercial γ-Al_2O_3 spheres 1 mm in diameter (Sasol Germany GmbH). Rh was deposited by incipient wetness impregnation technique, using 10 wt.% aqueous solution of $Rh(NO_3)_3$. The catalysts spheres were then calcined in air for 6 h at 600 °C [45]. The egg-yolk Rh catalyst, hereafter named catalyst "*B*", was synthesized starting from the preparation of stabilized Rh nanoparticles under Ar atmosphere at room temperature (T_{room}). Briefly, an aqueous solution containing $NaBH_4$ (the reducing agent) and the cationic surfactant HEAC16Br (used as protective agent for Rh metal particles) was quickly added under vigorous stirring to an aqueous solution of $Rh(NO_3)_3$. The obtained suspension was then stirred for 2 h to decompose the excess of reductant and finally $Al(NO_3)_3$ was added. When the complete dissolution of the salt was achieved, the precipitation of $Al(OH)_3$ was performed dropping the resulting system into NH_4OH solution. The formed gel was matured and then filtered. Several washing cycles were applied to remove the bromide ions from the surfactant [41]. The obtained precipitate was suspended in 2-propanol and refluxed for 5 h in order to stabilize the textural framework of the support. After filtration, the solid was dried at 120 °C overnight and calcined firstly at 500 °C for 5 h and then for 5 h at 900 °C. The carrier after calcination was composed of 50 wt.% γ-Al_2O_3 and 50 wt.% θ-Al_2O_3 [41]. Finally, the material was pressed, crushed and sieved to collect the fraction between 425 and 850 μm.

The morphology of as-prepared *A* and *B* catalysts was observed by FESEM (SEM FEI Quanta Inspect 200 LV apparatus) and HRTEM microscopy (Philips CM200 UT apparatus). The catalysts' BET surface area was measured by means of N_2 adsorption with an automated gas sorption analyzer (Micromeritics ASAP 2010C). Metal dispersion was estimated by H_2 chemisorption at 35 °C using a Micromeritics ASAP 2020C instrument. Prior to the experiments, the two catalysts were reduced at 750 °C for 2 h flowing H_2 (5%)/Ar (40 ml min^{-1}) and degassed at 750 °C for 5 min and at 400 °C for 3 h. The chemisorbed H_2 was determined by extrapolation to zero pressure of the linear part adsorption isotherm after removing the so-called reversible hydrogen adsorption ("double isotherm" procedure) and assuming a chemisorption stoichiometry Rh:H = 1:1.

The catalytic activity of the as-prepared catalysts was tested in a tubular reactor (Inconel® 601) composed of two coaxial pipes (the internal one 15 mm i.d. and 2 mm wall thickness) with a resulting jacket which contributed to the reactor thermal insulation [45]. The internal tube was covered with an oxidized layer of FeCrAlloy® to avoid contacts between reactive gases and the Inconel® surface wall [45], just to prevent any catalytic effect towards CPO reactions of Ni, present in the Inconel® alloy. The catalyst particles were arranged in a fixed bed placed between two porous inert regions. The upstream region was constituted by a quartz particles bed (to improve the CH_4/O_2 mixture by static mixing) followed by high thermal conductivity SiC particles (to provide both a shield for the radiant energy emerging from catalyst bed and, the pre-heating of the reagents fed at room temperature, thus exploiting the heat developed during the catalytic process). The downstream zone was a bed of low thermal conductivity quartz particles so as to reduce heat loss and allow a slower cooling of the outlet stream. The inlet (T_{in}) and outlet (T_{out}) catalyst bed temperatures were monitored by two suitably located thermocouples. The gas stream composition at the reactor outlet was monitored by a multiple gas analyzer (ABB) able to measure simultaneously H_2 (thermal conductivity module Caldos 17), $CO/CO_2/CH_4$ (infrared module Uras 14) and O_2 (paramagnetic module Magnos 106). The CPO reaction ignition was performed by heating the reactor, placed in a tubular oven, up to 920 °C and by feeding a T_{room} mixture of pure CH_4 and O_2 at O_2/CH_4 ratio equal to 0.5 (stoichiometric condition for MPO, reaction (2)). The feedstock stream was pre-heated by the hot particles bed region upstream the catalyst bed and once ignited, the reactor remained thermally self-sustained by the heat released from the exothermic reactions. The start-up procedure took about 1 min and then the O_2/CH_4 ratio was gradually increased to the operative desired value and maintained till to reach steady-state conditions. The chosen O_2/CH_4 ratio was 0.575, a value slightly above the stoichiometric one, which a previous research demonstrated to be the best one to maintain the $T_{reactor}$ in a proper range [45]. The feed flow rate was adjusted to obtain a WHSV between 120 and 470 Nl h^{-1} g_{cat}^{-1}. The as-prepared *A* and *B* catalysts were tested into the reactor in the following fixed bed structures (1.5 g of catalyst were always present in the bed, for a total length of about 2 cm):

i. *A* catalyst fixed bed only;
ii. *B* catalyst fixed bed only;
iii. *A* + *B* catalysts, 50 wt.%–50 wt.%, i.e., 1st bed *A* catalyst, 2nd bed *B* one;
iv. *B* + *A* catalysts, 50 wt.%–50 wt.%, i.e., 1st bed *B* catalyst, 2nd bed *A* one;
v. *A*/*B* catalysts mix, 50 wt.%–50 wt.%, i.e., a bed of a random *A* and *B* catalysts mixture.

3. Results and discussion

The characterization parameters of the basic catalysts are reported in Table 1. BET surface area values of the two catalysts are high and very similar, notwithstanding the complete different preparation methods used. This might suggest that the calcination step is able to reduce the differences related to the two preparation

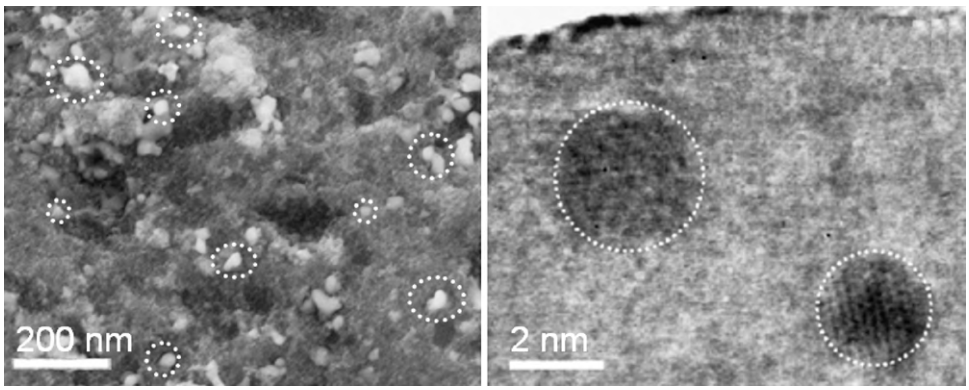

Fig. 1. FESEM image of the *A* catalyst and HRTEM image of the *B* catalyst; Rh clusters are enlightened.

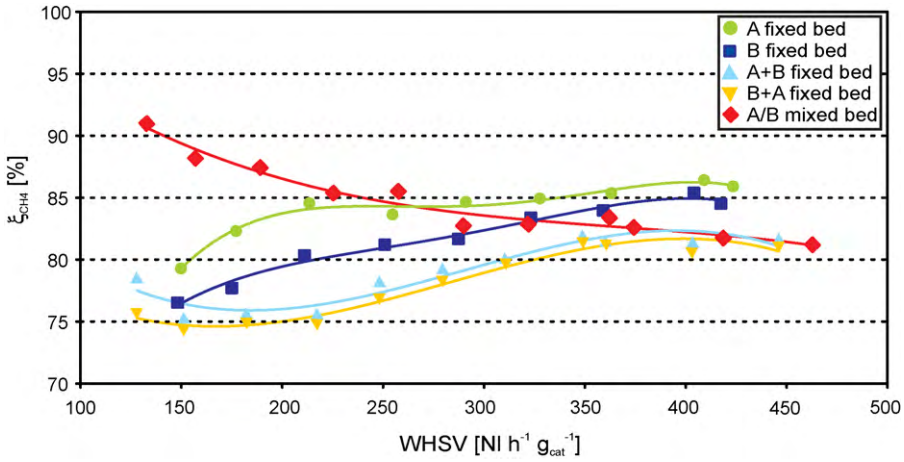

Fig. 2. CH_4 conversion vs. WHSV for various catalytic fixed beds.

routes. As expected, the *A* catalyst (egg-shell) showed 40% increase of both metal dispersion and accessible metal surface area compared to the catalyst *B* (egg-yolk), thanks to the presence of Rh nanoparticles exposed on the external surface of γ-Al_2O_3 spheres, whereas for *B* catalyst the Rh nanoparticles resulted embedded in the porous Al_2O_3 support. This is also evident from the FESEM/HRTEM images, reported in Fig. 1: FESEM analysis showed Rh particles up to 50 nm on *A* catalyst, enlightening also the presence of bigger clusters respect to the chemisorption analysis (mean particle diameter of 2.2 nm). On the contrary, FESEM analysis showed nothing on *B* catalyst, confirming thus the presence of only very small Rh clusters, not detectable with such a technique. Therefore, HRTEM investigations were applied to *B* catalyst: only Rh clusters from 2 to 4 nm, mainly fully embedded into the Al_2O_3, were detected. Notably, some partially embedded and some exposed Rh nanoparticles were observed as well.

Table 1
Basic characterization of the *A* and *B* catalysts.

	1 wt.% Rh–Al_2O_3 egg-shell (catalyst *A*)	1 wt.% Rh–Al_2O_3 egg-yolk (catalyst *B*)
BET area ($m^2\ g^{-1}$)	152	157
Pore volume (ml g^{-1})	0.45	0.77
Metal dispersion[a] (%)	49.3	35.5
Accessible metal surface area[a] ($m^2\ g^{-1}$)	2.17	1.57
Mean particle diameter[a,b] (nm)	2.2	3.1

[a] From H_2 chemisorption and by assuming a chemisorption stoichiometry Rh:H = 1:1.
[b] By assuming a spherical geometry for the metal particles.

The obtained results from the catalytic activity tests of the various fixed bed structures are reported in Fig. 2 as CH_4 conversion (ξ_{CH_4}), in Fig. 3 as H_2 (σ_{H_2}) and CO (σ_{CO}) selectivities and in Fig. 4 as fixed bed inlet (T_{in}) and outlet (T_{out}) temperatures. By comparing the two single catalyst beds, both *A* and *B* presented values of ξ_{CH_4}, σ_{H_2} and σ_{CO} increasing with WHSV; moreover, those of *A* were higher than those of the *B* one, and both became similar by increasing WHSV. The trends of the curves for both catalysts are very comparable: ξ_{CH_4} ranged from 79 to 86.5% for *A* and from 76.5 to 85% for *B* (Fig. 2); σ_{H_2} increased from 91.5 to 95% for *A* and from 89 to 94.5% for *B* (Fig. 3); σ_{CO} ranged from 87.5 to 92% for *A* and from 83 to 91.5% for *B* (Fig. 3). Therefore, as WHSV increased, ξ_{CH_4} became higher together with the selectivity of the products. This can be explained by assuming that the system operates under a transport-controlled regime. Increased ξ_{CH_4} are then associated with higher energy release and therefore higher temperatures, which favour syngas production: CO and H_2 formation is, in fact, favoured at high temperatures [17,20,22] in line with the obtained larger selectivity towards these products at higher WHSV.

Instead, by observing the T_{in}/T_{out} profiles of the two single fixed beds (Fig. 4), the trends were not the same: T_{in} for *A* was continuously diminishing with WHSV from 858 to 560 °C, whereas T_{out} decreased from 813 to 590 °C up to 290 Nl h^{-1} g_{cat}^{-1}, then increased reaching 710 °C at 410 Nl h^{-1} g_{cat}^{-1}. At low WHSV values T_{out} was lower than T_{in}, but overcame T_{in} at approx WHSV* = 330 Nl h^{-1} g_{cat}^{-1}; for WHSV > WHSV* T_{out} remained higher than T_{in}. On the contrary, *B* showed always a temperature level higher than that of *A*, moreover with T_{in} higher than T_{out} at all times; considering the trends, both temperatures firstly decreased with WHSV till 250–290 Nl h^{-1} g_{cat}^{-1} (T_{in} from 889 to 821 °C, T_{out}

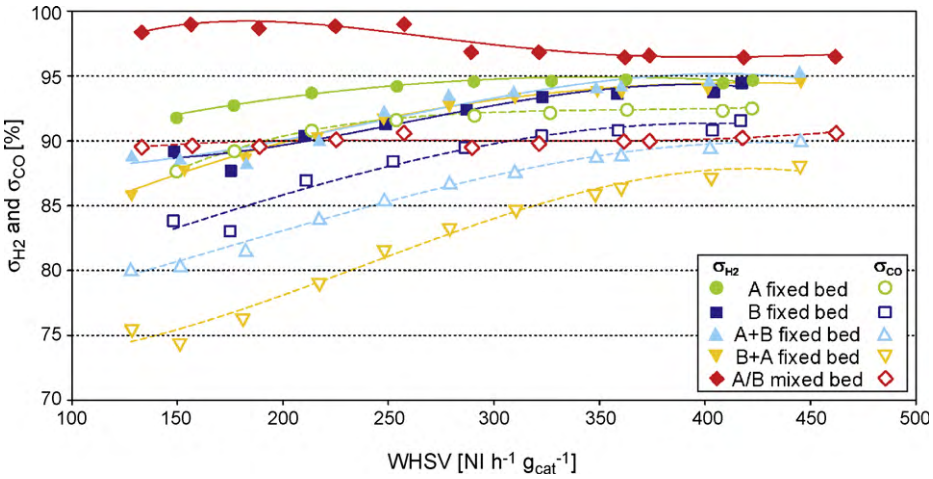

Fig. 3. H_2 and CO selectivity vs. WHSV for various catalytic fixed beds.

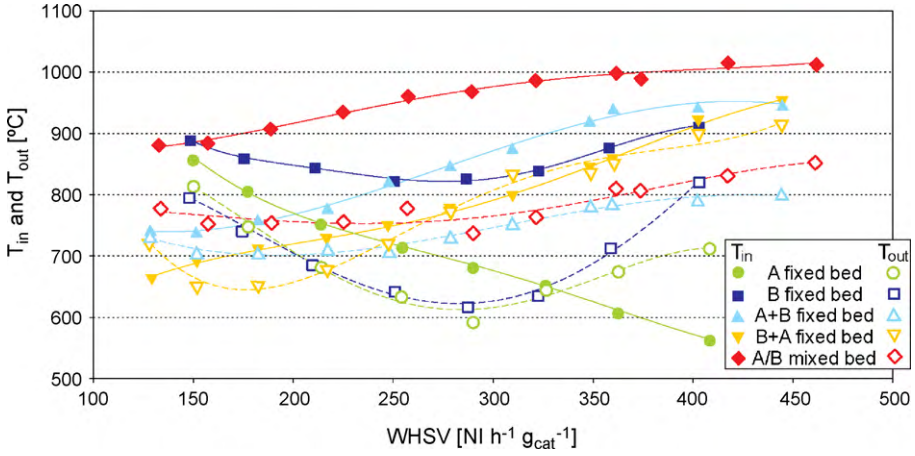

Fig. 4. Inlet and outlet temperatures vs. WHSV of the catalytic fixed bed for various catalytic fixed beds.

from 795 to 615 °C) and then increased with the feed rate (T_{in} to 913 °C, T_{out} to 820 °C). Results from literature [25–28,43,45] showed that in the inlet zone of the catalytic fixed bed prevailed the exothermic reactions of MTO/MPO, whereas in the outlet one the endothermic reactions of MSR/MDR/WGS took place. The presence of a peak temperature, moving along the fixed bed length varying WHSV, was interpreted as an evidence of the existence of an exo–endothermic reaction sequence.

To gain more insight, the measured T_{in} and T_{out} values of the catalytic *A* and *B* beds were reported for various WHSV in Fig. 5. By considering the difference between T_{out} and T_{in}, ΔT_{bed}, for each tested condition, ΔT_A was negative at low WHSV and positive at high WHSV whereas ΔT_B was always negative, and with absolute values bigger than ΔT_A. It is evident that the two catalysts worked at different thermal levels: at the same WHSV value, *B* temperatures were always higher than those of *A*, especially the inlet ones owing to the better particles heat conduction for the increased contact points in *B* bed, being the latter particles average size smaller than that of *A* (about 0.6 mm of *B* against 1 mm of *A*). This could suggest a prevailing of the MPO mechanism for *A* catalyst; T_{in} reduction increasing WHSV suggests larger difficulties in the inlet feedstock pre-heating by back radiation/conduction, since the lower reaction heat released by MPO is prevailingly capitalized by the endothermic reactions. Anyway, the system remains an autothermic one. On the contrary, the higher thermal level of catalyst *B* (the higher T_{in} recorded, always higher than T_{out} by increasing WHSV), could suggest that *B* performed better the MTO mechanism.

The different performance of the two catalysts could also be ascribed to the mass transfer controlling regime which for *B* catalyst involves, moreover, the intra-particle diffusion phenomenon; therefore, to develop the MDR/MSR reactions, CH_4 must reach the MTO products inside the *B* pores taking a longer time compared with that for *A* catalyst. Here, in fact, MTO products are available on the external surface of the particles. As a consequence, the endothermic reactions on *A* consume quickly the heat

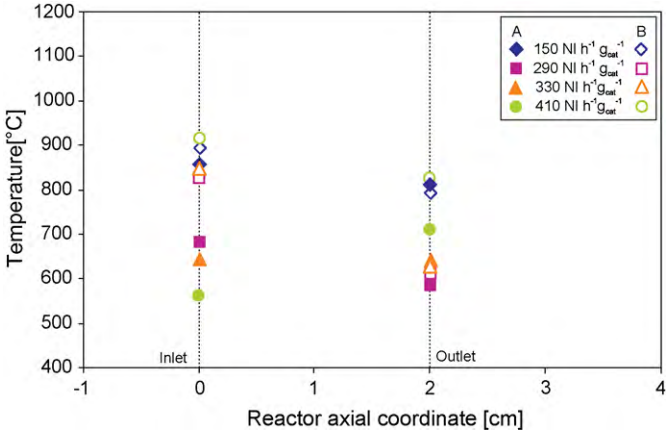

Fig. 5. T_{in} and T_{out} vs. the reactor axial coordinate for the catalytic fixed *A* and *B* beds at different WHSV values.

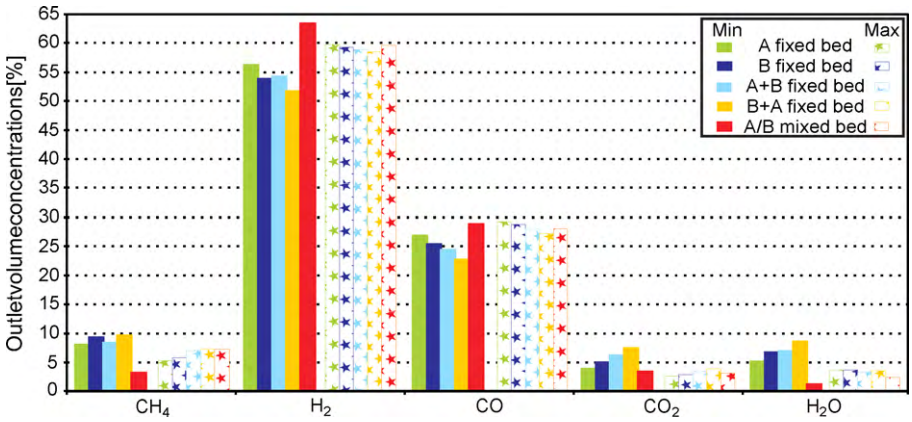

Fig. 6. Outlet volume wet concentrations at the minimum and maximum WHSV experimental values: 150/410 Nl h^{-1} $g_{cat}{}^{-1}$ for *A* and *B* beds; 130/450 Nl h^{-1} $g_{cat}{}^{-1}$ for *A* + *B*, *B* + *A* and *A*/*B* beds.

produced by CH_4 oxidation in agreement with the lower temperature level measured experimentally. For *B* catalyst the exothermic and endothermic zone should be presumably more markedly in series than for *A* catalyst, where a merge seems to be more plausible.

In addition, at the end of the tests, *A* catalyst spheres appeared gray, as covered by coke particles, whereas this effect did not happen to *B* catalyst: coke formation (Eq. (6)) is, in fact, favoured at lower thermal level, as happened with *A* catalyst. This occurrence also seems to suggest that egg-shell structure favoured the MPO pathway, whereas egg-yolk the MTO one.

The different behaviour of the two catalysts could also be a consequence of the different Rh cluster size exposed to the reactive gas mixture: *A* catalyst showed Rh clusters size from 2 to 50 nm, whereas the nanoclusters of *B* catalyst were approx. 3 nm (Table 1 and Fig. 1). Many studies on model metal surface suggested that C–H bond activation is the kinetically relevant step in CH_4 conversion to H_2–CO mixtures [35,36], and C–H bond dissociation occurs faster on step and kink sites (very small Rh nanoclusters) than on terrace sites (bigger Rh clusters) [32,34]. In particular, MDR mechanism is structure-sensitive on Rh/Al_2O_3: the turnover rates depended significantly on Rh crystallite size (1–7 nm) [33] and the specific activity increased with increasing Rh dispersion on the Al_2O_3 carrier, suggesting that coordinatively unsaturated Rh surface atoms, prevalent in small clusters, are more active [31]. This should explain why sample *B* performed better the MTO mechanism.

By analyzing the performance of the double-catalyst beds, the best ξ_{CH_4} results were obtained with *A*/*B* mix at low-medium WHSV, but with a decreasing trend increasing WHSV: ξ_{CH_4} equal to 91% at the minimum and to 81% at the maximum WHSV tested value. At the latter condition, ξ_{CH_4} resulted practically the same as for *A* + *B* (ξ_{CH_4} increased from 78.5 to 81.5% at the maximum tested WHSV) and *B* + *A* beds (ξ_{CH_4} increased from 75.5 to 81% at the maximum tested WHSV). *A* + *B* and *B* + *A* beds showed always lower ξ_{CH_4} values compared to *A* or *B* alone. Concerning σ_{H_2}, instead, the *A*/*B* mix demonstrated a superior performance, always over 96%, with a very high thermal level (T_{in} was always the highest compared to all the examined configurations), whereas the best single catalyst bed *A* was characterized by σ_{H_2} values between 91.5 and 95%. The overall performance of *A* + *B* and *B* + *A* beds worsened, probably due to the higher occurrence of MTO, especially in *B* + *A* configuration. This was also perceived by the higher T_{out} values (higher thermal level) in *B* + *A* compared to *A* + *B* and *A*/*B* mix configurations, obtained for WHSV higher than about 250–275 Nl h^{-1} $g_{cat}{}^{-1}$. On the other hand, the lower σ_{CO} values (i.e., higher CO_2 concentrations in the outlet stream) for *B* + *A* bed could be considered as an index of higher MTO occurrence, favoured by the first part of the fixed bed, where *B* catalyst was present. This was in agreement with the observations done for the single *A* and *B* fixed beds.

From the outlet stream concentrations (see Fig. 6, reporting only the ones for the min and max WHSV), it is possible to estimate the H_2 (Y_{H_2}) and CO (Y_{CO}) yields (calculated as the product between

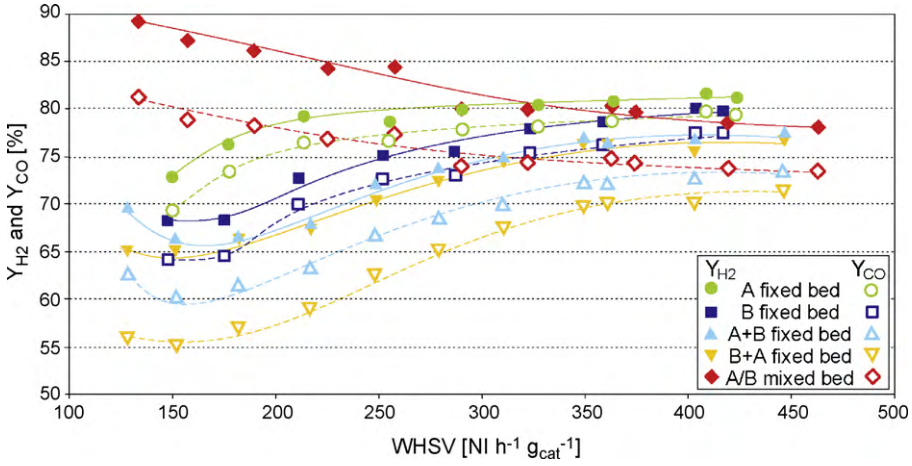

Fig. 7. H_2 and CO yields vs. WHSV for the various catalytic fixed beds.

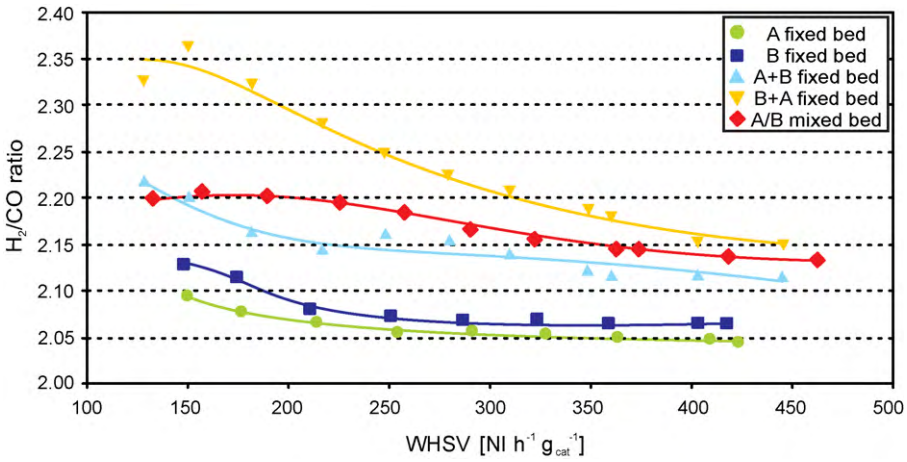

Fig. 8. H_2/CO ratio vs. WHSV for the various catalytic fixed beds.

ξ_{CH_4} and σ_{H_2} or σ_{CO}, respectively), as well the H_2/CO ratio; the corresponding values are reported in Figs. 7 and 8, respectively. It is worth noting that H_2 and CO yields increased for *A*, *B*, *A* + *B* and *B* + *A* fixed beds by varying WHSV from the minimum to the maximum value, whereas for the mixed bed *A*/*B* the trend was reverse. In particular, the lower decrease of CO yield compared to the H_2 one (as a consequence of the σ_{CO} trend which remained constant by varying WHSV, whereas ξ_{CH_4} and σ_{H_2} decreased, see Figs. 2 and 3) led to a major CO concentration at the reactor outlet, probably due to the effect of the reverse WGS side reaction. The H_2/CO ratio, which is equal to 2 when only MPO reaction occurs, increased in the following order, at constant WHSV value: $A < B < A + B < B + A$ (see Fig. 8), denoting again a larger occurrence of MTO over MPO reaction for the *B* catalyst compared to *A* and for the mixed beds. The mixed bed *A*/*B* presented intermediate values between *A* + *B* and *B* + *A*. For all the catalytic bed structures, H_2/CO decreased as WHSV increased, favoured to some extent from the MPO mechanism. It is widely demonstrated, in fact, that syngas production is favoured both kinetically and thermodynamically at high temperature [26,45]: when WHSV increased, mass and heat transfer improved within the fixed bed, thus establishing the increase in ξ_{CH_4} that in turn enhanced the system temperatures and pushed up the product yields [43]. Perhaps, an increase of WHSV could favour in some extent a reaction mechanism switch from MTO and reforming reactions, at low WHSV, to a direct MPO reaction, at high WHSV.

Considering the problem of coke formation, *A*/*B* and *B* + *A* beds did not show appreciable coke formation, whereas *A* + *B* showed coke formation limited to *A* layer. This is also in agreement with the observations done with the single fixed beds: a higher exothermicity of the system helped in limiting coke formation.

A good compromise was reached with *A*/*B* mix: probably the close position of *A* and *B* particles all along the bed length was the key-factor to balance both MPO and MTO. The mutual interaction of MTO and MPO gave, in fact, the right local amount of heat, limiting the increase of the T_{out}, i.e. without incurring in high *T* increase as happened where largely MTO was involved. Moreover, the presence of Rh clusters both on the surface (*A* catalyst) and inside the pores (*B* catalyst) led to a synergetic balance of the exothermic and endothermic zones, especially at low-medium WHSV, giving the highest ξ_{CH_4}, $\sigma\sigma_{H_2}$ σ_{CO}, Y_{H_2}, Y_{CO} values, also if with not very favourable H_2/CO ratio.

4. Conclusions

CH_4 catalytic partial oxidation represents an attractive process for syngas production. The present work investigated, in the WHSV range from 120 to 450 Nl h^{-1} g_{cat}^{-1}, five different 1 wt.% Rh-based fixed bed structures using egg-shell (*A* catalyst) and egg-yolk (*B* catalyst) Al_2O_3 particles. The best performances in term of CH_4 conversion, H_2 and CO selectivities and H_2 and CO yields (also if with not the H_2/CO ratio closest to 2), together with no coke formation, were obtained with an intimate mechanical mixture of *A*- and *B*-type catalysts at WHSV values of 150–300 Nl h^{-1} g_{cat}^{-1}.

Acknowledgements

Politecnico di Torino, Università di Trieste, CNR-ICCOM, INSTM and FISR2002 are gratefully acknowledged for financial support. Helpful discussions with Professor Guido Saracco (Politecnico di Torino) are acknowledged.

References

[1] J.N. Armor, Appl. Catal. A 176 (1999) 159.
[2] L. Carrette, K.A. Friedrich, U. Stimming, Fuel Cells 1 (2001) 5.
[3] V.R. Choudhary, V.H. Rane, A.M. Rajput, Appl. Catal. A: Gen. 162 (1997) 235.
[4] V.R. Choudhary, A.M. Rajput, B. Prabhakar, Catal. Lett. 15 (1992) 363.
[5] V.R. Choudhary, A.M. Rajput, V.H. Rane, Catal. Lett. 16 (1992) 269.
[6] A.T. Ashcroft, P.D.F. Vernon, M.L.H. Green, Nature 344 (1990) 319.
[7] D. Dissanayake, M.P. Rosynek, K.C. Kharas, J.H. Lunsford, J. Catal. 132 (1991) 117.
[8] W.J.M. Vermeriren, E. Blomsma, P.A. Jacobs, Catal. Today 13 (1992) 427.
[9] S.C. Tsang, J.B. Claridge, M.L.H. Green, Catal. Today 23 (1995) 3.
[10] D. Dissanayake, M.P. Rosynek, J.H. Lunsford, J. Phys. Chem. 97 (1993) 3644.
[11] D.A. Hickman, L.D. Schmidt, Science 259 (1993) 343.
[12] D.A. Hickman, L.D. Schmidt, Catal. Lett. 17 (1993) 223.
[13] L.D. Schmidt, M. Huff, Catal. Today 21 (1994) 443.
[14] Y. Matsumura, J.B. Moffat, Catal. Lett. 24 (1994) 59.
[15] S.S. Bharadwaj, L.D. Schmidt, Fuel Process. Technol. 42 (1995) 109.
[16] O. Deutschmann, L.D. Schmidt, Proc. Comb. Inst. 27 (1998) 2283.
[17] A.S. Bodke, S.S. Bharadwaj, L.D. Schmidt, E. Ranzi, Science 285 (1999) 712.
[18] O. Deutschmann, L.D. Schmidt, AIChE J. 44 (1999) 2465.
[19] D.K. Zerkle, M.D. Allendorf, M. Wolf, O. Deutschmann, J. Catal. 196 (2000) 18.
[20] L. Basini, A. Guarinoni, A. Aragno, J. Catal. 190 (2000) 284.
[21] O. Deutschmann, R. Schwiedernoch, L.I. Maier, D. Chatterjee, Stud. Surf. Sci. Catal. 136 (2001) 251.
[22] L. Basini, K. Aasberg-Petersen, A. Guarinoni, M. Ostberg, Catal. Today 64 (2001) 9.
[23] K.L. Hohn, L.D. Schmidt, Appl. Catal. A: Gen. 211 (2001) 53.
[24] L.D. Schmidt, E.J. Klein, C.A. Leclerc, J.J. Krummenakcher, K.N. West, Chem. Eng. Sci. 58 (2003) 1037.
[25] I. Tavazzi, A. Beretta, G. Groppi, P. Forzatti, Stud. Surf. Sci. Catal. 147 (2004) 163.
[26] M. Maestri, A. Beretta, G. Groppi, E. Tronconi, P. Forzatti, Catal. Today 105 (2005) 709.
[27] I. Tavazzi, A. Beretta, G. Groppi, P. Forzatti, J. Catal. 241 (2006) 1.
[28] A. Beretta, T. Bruno, G. Groppi, I. Tavazzi, P. Forzatti, Appl. Catal. B: Environ. 70 (2007) 515.
[29] J.B. Claridge, M.L.H. Green, S.C. Tsang, A.P.E. York, A.T. Ashcroft, P.D. Battle, Catal. Lett. 22 (1993) 299.
[30] A.P.E. York, T.C. Xiao, M.L.H. Green, Top. Catal. 22 (2003) 345.
[31] Z.L. Zhang, V.A. Tsipouriari, A.M. Efstathiou, X.E. Verykios, J. Catal. 158 (1996) 51.
[32] K. Klier, J.S. Hess, R.G. Herman, J. Chem. Phys. 107 (1997) 4033.
[33] H.Y. Wang, E. Ruckenstein, Appl. Catal. A: Gen. 204 (2000) 143.
[34] Z. Liu, P. Hu, J. Am. Chem. Soc. 125 (2003) 1958.

[35] J. Wei, E. Iglesia, J. Catal. 224 (2004) 370.
[36] J. Wei, E. Iglesia, J. Catal. 225 (2004) 116.
[37] E. Finocchio, G. Busca, P. Forzatti, G. Groppi, A. Beretta, Langmuir 23 (2007) 10419.
[38] V. Dal Santo, C. Mondelli, V. De Grandi, A. Gallo, S. Recchia, L. Sordelli, R. Psaro, Appl. Catal. A: Gen. 346 (2008) 126.
[39] A. Beretta, A. Donazzi, G. Groppi, P. Forzatti, V. Dal Santo, L. Sordelli, V. De Grandi, R. Psaro, Appl. Catal. B: Environ. 83 (2008) 96.
[40] I. Tavazzi, A. Beretta, G. Groppi, M. Maestri, E. Tronconi, P. Forzatti, Catal. Today 129 (2007) 372.
[41] T. Montini, A.M. Condò, N. Hickey, F.C. Lovey, L. De Rogatis, P. Fornasiero, M. Graziani, Appl. Catal. B: Environ. 73 (2007) 84.
[42] L. De Rogatis, T. Montini, V. Gombac, M. Cargnello, P. Fornasiero, in: W.V. Prescott, A.I. Schwartz (Eds.), Nanorods, Nanotubes and Nanomaterials Research Progress, Nova Science Publishers, New York, 2008 , p. 71 (Chap. 2).
[43] M. Bizzi, L. Basini, G. Saracco, V. Specchia, Ind. Eng. Chem. Res. 42 (2003) 62.
[44] K. Hori, H. Matsune, S. Takenaka, M. Kishida, Sci. Technol. Adv. Mater. 7 (2006) 678.
[45] S. Specchia, G. Negro, G. Saracco, V. Specchia, Appl. Catal. B: Environ. 70 (2007) 525.